2013 International Nuclear Atlantic Conference - INAC 2013
Recife, PE, Brazil, November 24-29, 2013
ASSOCIAÇÃO BRASILEIRA DE ENERGIA NUCLEAR - ABEN
ISBN: **978-85-99141-05-2**

COLLIMATION EFFECTS ON THE RADIATION DETECTORS IN THE iCT IMAGE QUALITY

Diego Vergaças de Sousa Carvalho[1]*, Rodrigo Kirita[1], Carlos Henrique de Mesquita[1], Eric Oliveira Ferreira[2], Carlos Costa Dantas[2], Margarida Mizue Hamada[1]

[1] Nuclear and Energy Research Institute (IPEN / CNEN - SP)
Av. Professor Lineu Prestes 2242
05508-000 São Paulo, SP, Brasil
*dvcarvalho@usp.br

[2] Department of Nuclear Energy (DEN / UFPE)
Av. Professor Luiz Freire, 100
Recife, PE, Brasil

ABSTRACT

This work studies the collimation effect in radiation detectors on the image quality of the iCT scanner, in which the path traversed by radiation beams is similar to a fan. The collimators were made of lead, 5 cm deep and 12 cm high, with rectangular holes (slits) of 2 x 5 mm, 4 x 10 mm (width x height) and circular hole of 5 mm diameter. The matrix images reconstructed from the data obtained with these collimation holes are presented. The spatial resolution of the image depends on the geometry of the collimator. One of the major advantages of narrow beam transmission tomography is the so-called hard field property. This property is capable of producing high quality images, though it decreases the count value and it takes a longer time. In contrast, a large collimation diameter produces a fuzzy image but with a faster scanning time. Moreover, the enlargement of the aperture from 2 x 5 mm to 4 x 10 mm barely affects the image quality. The aperture from 4 x 10 mm and 5 mm diameter presented similar quality image.

Key Words: Industrial Computed Tomography, Radiation Measurements, Collimator, Image Quality.

1. INTRODUCTION

For the last years, industrial computed tomography (iCT) in Brazil has had its application in non-destructive testing, for scientific studies. Today, the interest of a wide range of industries, such as chemical and oil sectors in the use of computed tomography began to appear in large number, for improving design, operation and troubleshooting of industrial processes. Computerized tomography for multiphase processes is now a promising technique and has been studied for advanced research centers [1-5].

The iCT systems based on transmission employ an array of encapsulated radioactive sources and detectors placed in opposite sides of the targeted object. [5-8]. First generation tomography systems consist of a source emitting a collimated radiation linear beam and a

ISBN: **978-85-99141-05-2**

radiation detector (Figure 1 A). The source-detector system moves in opposite sides of the object, measuring the attenuation of radiation at each position.

In the second generation iCT systems, a set of detectors is placed opposite to a set of radioactive sources, moving (source and detector) around the object under study, providing a number of projections equal to the number of detectors (Figure 1 B). Sometimes, these second generation systems, also, use multiple radioactive sources in order to reduce the analysis time of the system.

In the tomography of third generation, the source is collimated so that the path crossed by beams is similar to a fan (Figure 1 C). The system moves around the targeted object, obtaining a particular view for an "x" position of the source-detector array. In this type of system, several sources and arrays of multiple detectors may be used.

Finally, the so-called fourth-generation iCT systems use a fixed array of detectors (a large number of detectors mounted on a fixed ring) and a radioactive source that moves around the object (Figure 1 D). Records of any measurements are from the detector, representing a view of the object. However, all iCTs are constituted, basically, of same parts: radioactive sources; radiation detectors; a data acquisition system and a suitable computer.

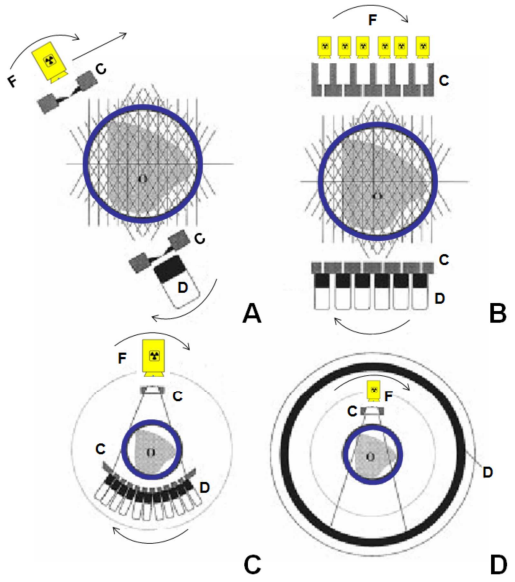

Figure 1: (A) translation - rotation of a beam in parallel (first generation), (B) translation - rotation of multiple sources in parallel (second generation), (C) rotation of a fan-beam (third generation), (D) detector fixed - rotation source (fourth generation). D: detectors; F: source C: collimator, O: object of study .

Unlike the standard aspect of the iCT for medical application, tomography systems for industrial process applications should be adapted to the different size and geometry of objects usually placed in an aggressive environment, which contains flammable superheated or corrosive materials, and may be, eventually, subject to high internal pressure: all these factors bring in many difficulties for setting iCT devices around the objects (Figure 2) [1, 9].

ISBN: **978-85-99141-05-2**

Therefore, the development of special iCTs is required, inhibiting its production in large scale. In addition, the industrial systems involve dynamic processes and contain mixtures of solids, liquids and gases where iCT is an excellent option to see the phases distribution inside the vessels [2-5, 10]. In other words, it is necessary to develop a tomographic system suitable for each purpose in industry [4, 9].

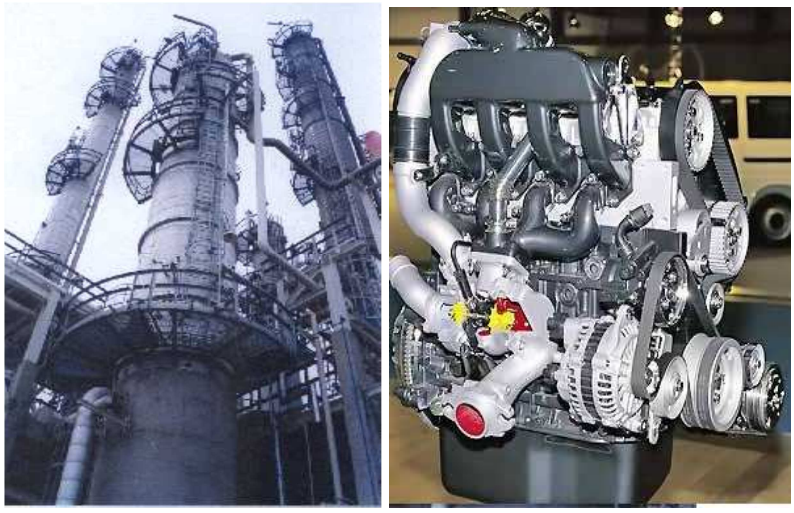

Figure 2: Illustration of systems with multiphase processes in industry

At the IPEN laboratory, a third generation computed tomography system was developed. In this configuration, NaI(Tl) multi-detectors are positioned on an concentric arc to a gamma source, which can be ^{60}Co, ^{75}Se, ^{137}Cs and /or ^{192}I. The size of the detector array is sufficiently large so that the entire object is within the detector field view at all times. The source and the detector array remain stationary with respect to each other, while the entire apparatus rotates around the object. Suitable results have been found in experiments using developed iCT scanners; however, in the design of an industrial tomography system, it is important to seek and study parameters for its improvement and to meet the requirement of the high temporal resolution and high detection efficiency. One of the important parameters that should be investigated is the geometry of the radiation beam, since the process interaction based on gamma rays by different means produces a number of secondary radiations. The presence of this secondary radiation strongly influences the overall process of the interaction of gamma radiation and diffusion, because these scattered radiations may reach the detector and be counted. To avoid the influence of this phenomenon, the most important requirement is to use a narrow-beam geometry, in which the photons, which are incoherently or coherently backscattered by a small angle, are prevented from reaching the detector [11]. The use of radiation absorber collimators can prevent this problem. The collimators are made with materials that attenuate gamma rays, such as lead and tungsten, with narrow openings (windows) that select gamma photons in a small solid angle on the face of the detector. For evaluating the collimation effect, lead collimators of different windows were used to carry out the tomographic measurements.

2013 International Nuclear Atlantic Conference - INAC 2013
Recife, PE, Brazil, November 24-29, 2013
ASSOCIAÇÃO BRASILEIRA DE ENERGIA NUCLEAR - ABEN
ISBN: **978-85-99141-05-2**

2. EXPERIMENTAL PROCEDURE

A third generation computed tomography was developed for industrial applications at the CTR-IPEN/CNEN-SP [8-10]. In this work, an array of five NaI(Tl) detectors of 50 x 50 mm (diameter x height) were positioned in a concentric arc sources of gamma ray and the set of collimators and detectors around the object to be analyzed. In order to increase the number of projection measurements in one view of the column, the number of detectors in the arc was effectively increased by using a collimator that moves across the detector arc (Figure 3). The whole assembly of the detectors and the radiation source are mounted on a gantry capable of being rotated around the object through a stepper motor controlled by a host computer. In this work, five NaI(Tl) detectors were used and individually collimated with lead. Three types of the collimators were used in order to evaluate the collimation effect on the radiation detectors. Each collimator was made of lead, 50 mm deep and 120 mm high, with rectangular holes (slits) of 2 x 5 mm and 4 x 10 mm (width x height) and circular hole of 5 mm diameter, as illustrated in figure 4. ^{75}Se and ^{137}Cs radioactive sources were used for tomographic measurements.

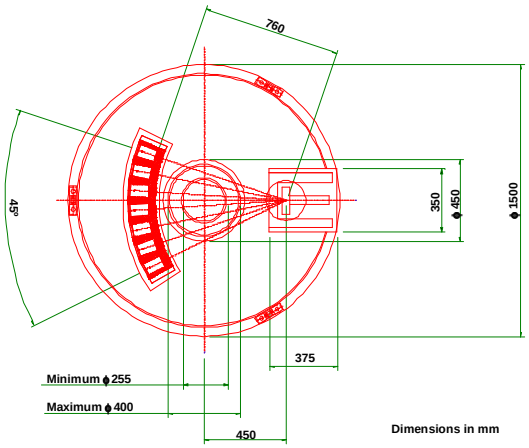

Figure 3: Top view drawing of the iCT used.

A B

C

Figure 4: Photos of the collimators developed in this work

ISBN: **978-85-99141-05-2**

Previously, the five detectors were adjusted using a ^{137}Cs source. The gain of each detector amplifier was adjusted in order to maintain similar spectrum profile. After that, measurements for each detector were carried out, using three different collimators and two different radioactive sources (^{75}Se (97 keV, 121 keV, 136 keV, 265 keV, 280 keV and 400 keV and 137Cs (662 keV)), separately. After, the preliminary adjustments, the ^{75}Se and ^{137}Cs sources were placed together into a lead shield to perform the iCT measurements.

A multiphase phantom was designed and prepared in order to be able of varying the proportions of the phases (gas, liquid or solid). This phantom consists of a 165 mm diameter polymethyl methacrylate (PMMA) solid containing three holes, being one filled with a steel plug, another with an aluminum plug and the third one empty, as illustrated in Figure 5. The idea was to switch the gas and liquid phases, while maintaining the solids fixed.

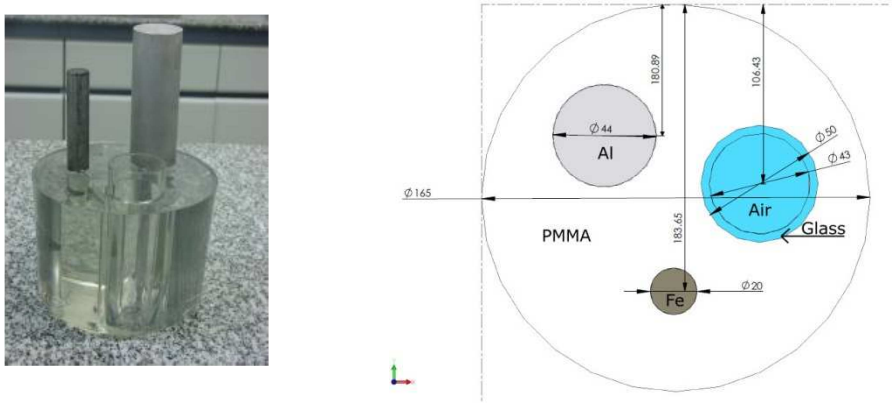

Figure 5: Picture of the multiphase phantom

The array of five NaI(Tl) detectors and two different radioactive sources, ^{137}Cs and ^{75}Se, were placed together into a single lead collimation system. They were placed on the rotatable gantry and the phantom, shown in (Figure 5), was installed in the center between the array of detectors and the source. The gantry can be rotated around the axis of the phantom by a stepping motor that is controlled through a microprocessor. The size of the array of detectors is sufficiently large so that the entire phantom was within the field of view of the detectors all the time. Moreover, the whole assembly can be moved in the axial direction along the phantom to perform a scan at different axial levels of the phantom. (Figure 6) shows an illustration of the third generation iCT with the phantom in the center of the gantry. The data acquisition board and the mechanical control used were developed at CTR/IPEN also [9, 10].

ISBN: **978-85-99141-05-2**

Figure 6: Set-up of the third generation iCT.

The iCT scans were carried out, rotating at 360°, stepwise of 6°, the table together with the source and detectors around the column, generating 60 views. The movement of the detector–collimator assembly was controlled by another stepper motor; the movement step for each collimator was different. For rectangular holes (slits) of 2 x 5 mm collimator, the assembly generated 47 ray projections per each detector or 235 (47 x 5) ray projections per view; totalizing 14100 (235 x 60) ray projections per image. For rectangular holes (slits) of 4 x 10 mm collimator, the assembly generated 23 ray projections per each detector or 115 (23 x 5) ray projections per view; totalizing 6 900 (235 x 60) ray projections per image. Finally, for circular hole of 5 mm diameter the assembly generated 18 ray projections per each detector or 90 (18 x 5) ray projections per view; totalizing 5 400 (90 x 60) ray projections per image.

3. RESULTS AND DISCUSSION

The typical energy spectra of ^{75}Se (97 keV, 121 keV, 136 keV, 265 keV, 279 keV and 400 keV) and ^{137}Cs (662 keV) [16, 17, 13] obtained for the detectors collimated at different slits: rectangular holes (slits) of 2 x 5 mm and 4 x 10 mm (width x height) and circular hole of 5 mm diameter are shown in (Figure 7). As it can be observed in these Figures the Compton region of ^{137}Cs overlaps the 400 keV ^{75}Se photopeak, while the 97 keV, 121 keV, 136 keV ^{75}Se photopeaks are superimposed among them. The photopeak at 265 kev can be distinguished from the photopeak 279 kev only for the collimator 2 x 4 mm aperture (Figure 4 A). A slight peak was observed in the spectrum. For the other two collimators an overlap between the two peaks 265 and 279 keV was found (Figure 4 B and 4 C). A good linear correlation between the different energies of gamma radiation sources (^{75}Se and ^{137}Cs) and channel number was found for the three types of collimators, as shown in (Figure 7).

ISBN: **978-85-99141-05-2**

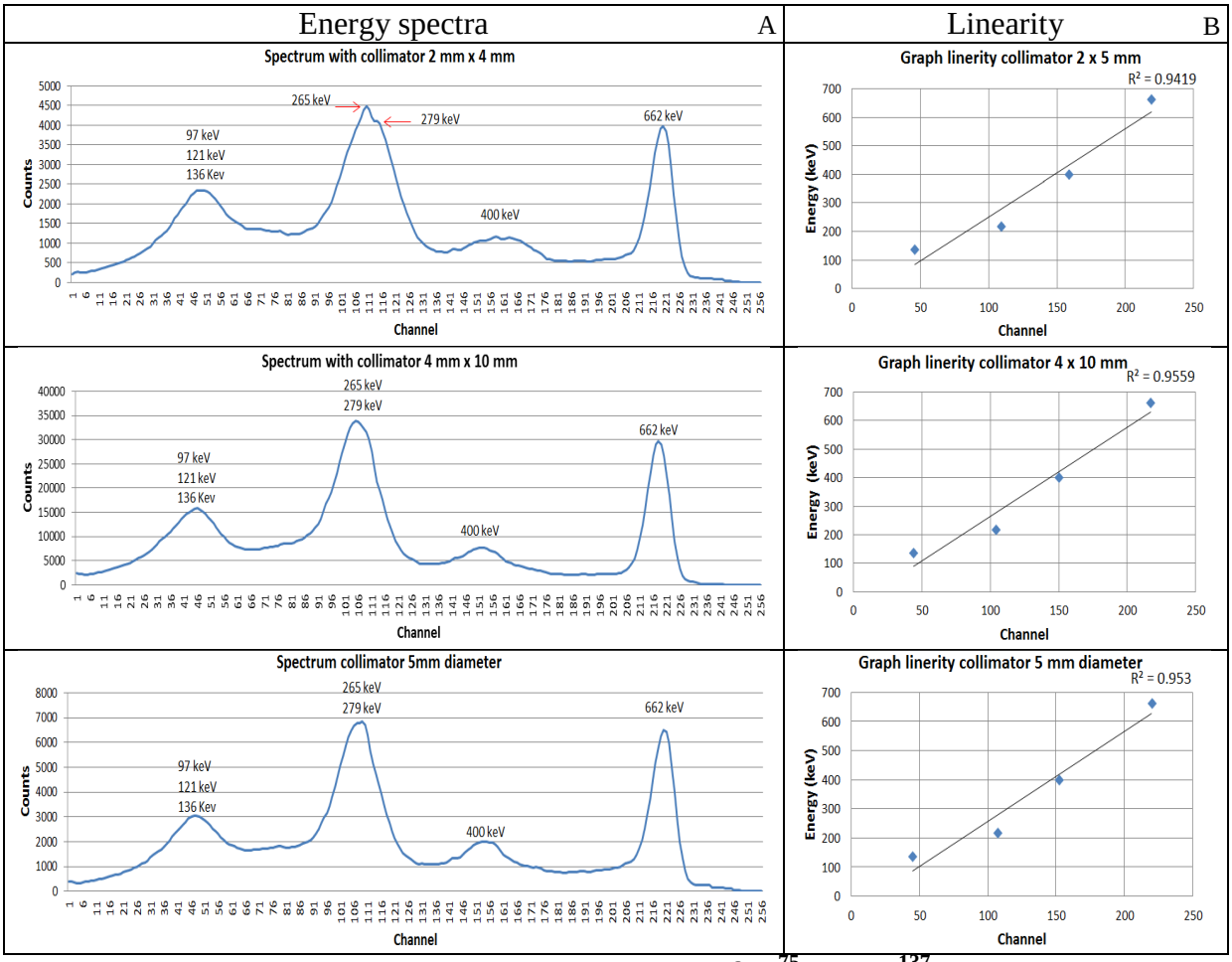

Figure 7. Graph energy spectra and graph linearity for ^{75}Se and ^{137}Cs sources measured simultaneously.

The reconstruction algorithms used was the Simultaneous Multiplicative Algebraic Reconstruction Technique with Correction (SMART) techniques and was implemented in VB platforms. [12, 14, 15]

The tomographic measurements were carried out selecting only the region between the 265 keV ^{75}Se photopeak and 622 keV ^{137}Cs photopeak. Figure 7 shows the reconstructed tomograms of PMMA solid phantom containing three holes, being one filled with a steel plug, another with an aluminum plug and the third one empty, at ~ 272keV (average energy between 265 and 279 keV) and 662 keV for the three different collimators. The results were reconstructed in 141x141 pixels images and 256 x 256 pixel images.

ISBN: **978-85-99141-05-2**

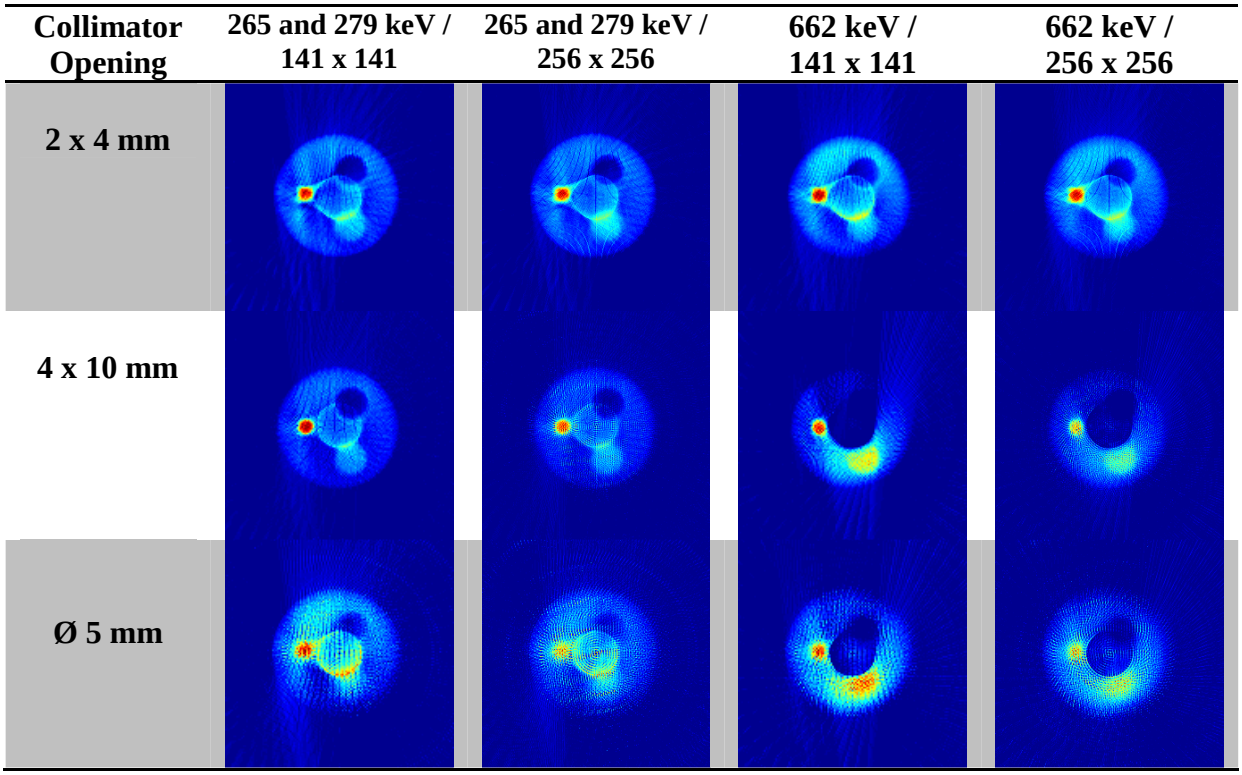

Figure 8 – Reconstructed images for different collimator slits at 265, 279 keV and 622keV.

As it can be observed in Figure 8, the images obtained using 2 x 4 mm collimator slit present an enhanced resolution in relation to 5 x 10 mm slit and circular hole of 5 mm diameter. As the opening dimension increased the image definition worsened. The best image resolution obtained by smaller aperture collimator can be explained by the greater amount of projected rays (view). For 2 x 4 mm collimator slit, the assembly generated 47 ray projection per each detector or 235 (47 x 5) ray projection per view, totalizers 14100 (235 x 60) ray projection per image, while for 4 x 5 mm collimator, the assembly generated 23 ray projections per each detector or 115 (23 x 5) ray projections per view; totalizing 6 900 (115 x 60) ray projections per image. Finally, for circular hole of 5 mm diameter the assembly generated 18 ray projections per each detector or 90 (18 x 5) ray projections per view; totalizing 5 400 (90 x 60) ray projections per image.

On the other hand, better images were obtained for 272 keV ^{75}Se energy compared to 662 keV ^{137}Cs, since it presents artifacts in the center of the image due to the high attenuation coefficient (Table 1). Both, 141 x 141 pixels images and 256 x 256 pixel images presented no significant difference concerning the image quality. The best image was found for tomographic measurement carried out with 2 x 4 mm slit collimator and 273 keV from ^{75}Se source, however, the time spent for the measurement is longer, as summarized in Table 2.

ISBN: **978-85-99141-05-2**

Table 1: Material Mean Densities and Attenuation Coefficient of ^{75}Se and ^{137}Cs. [16, 17, 18]

Material	Density (g/cm³)	Attenuation coefficient ^{75}Se (μ)	Attenuation coefficient ^{137}Cs (μ)
Polymethyl methacrylate	1.18	0.219	0.099
Aluminum	2.697	0.290	0.203
Iron	7.874	0,944	0.605
Air	1.225×10^{-3}	1.200×10^{4}	1.060×10^{4}

Table 2: Number of ray projection per image and time spent for TC measurement.

Collimator	Points	Time (minutes)
2 x 5 mm	14,100	470
4 x 10 mm	6,900	230
5 mm Ø	5,400	180

4. CONCLUSIONS

The best image was obtained with the collimator of rectangular holes (2 x 5 mm slits) compared to that with 5 x 10 mm and, circular hole of 5 mm diameter, probably due to its greater quantity of 14,100 ray projections per image in relation to 6,900 and 5,400 ray projections per image, respectively. Smaller collimation slits produced images of higher quality, although decreasing the counting value and increasing the iCT measurement time. On the other hand, the enlargement of the slits, from 2 x 5 mm to 5 x 10 mm and 5 mm diameter, affected the image quality, but a faster scanning time was reached. The iCT measurement times were 470, 230, and 180 minutes for 2 x 5 mm, 5 x 10 mm and 5 mm diameter, respectively. For the materials used in this work (Al, Fe, Air and PMMA), the best image quality was obtained for the 265 keV from the 75Se source compared to images obtained with 662 keV from 137Cs.

ACKNOWLEDGMENTS

The author would to express their gratitude to the FAPESP for the financial support to carried out the present work. They are also grateful for the research grant and scholarship for undergraduate and postgraduate students.

REFERENCES

1. S. B. Kumar, J. Chaouki, F. Larachi, M. P. Dudukovic, *Computer-assisted gamma and X-ray tomography: Application to multiphase flow*. *In Non-Invasive Monitoring of Multiphase Flows*; ´, M. P., Eds.; Elsevier: Amsterdam, The Netherlands, 1997; Chapter 2, p 48.

ISBN: **978-85-99141-05-2**

2. S. B. Kumar, M. P. Dudukovic, Gas holdup in bubble columns at elevated pressure via computed tomography. *Int. J. Multiphase Flows*, v. **27**, pp.929-946, 2001.

3. J. Ismaila, J. C. Gamiog, Tomography for rmulti-phase flow measurement in the oil industry. *Flow Measurement and Instrumentation*, vol. 16, pp. 145-155, 2005.

4. P. A. S. Vasquez, C. H. Mesquita, M. M. Hamada, Methodological Analysis of Gamma Tomography System for Large Random Packed Columns. *Applied Radiation and Isotopes*, v. **68**, p. 658-661, 2010.

5. *IAEA-TECDOC-1589*, Industrial Process Gamma Tomography, Viena, Maio 2008.

6. P. A. S. Vasquez, Análise de sistemas multifásicos utilizando tomografia computadorizada gama monoenergética e polienergética. 2008 *Tese (Doutorado) – IPEN-USP*, São Paulo.

7. J. Chaouko, F. Larachi, M. P. Dudukovic, Noninvasive Tomographic and Velocimetric Monitoring of Multiphase Flows. *Ind. Eng. Chem. Res.*, v. **36**, p. 4476-4503, 1997.

8. G. A. Johansen, P. Jackson, *Radioisotope Gauges for Industrial Process Measurements*. 2004 John Wiley & Sons, Ltd. ISBN 0-471-48999-9.

9. W. A. P. Calvo, M. M. Hamada, F. E. Sprenger, P. A. S. Vasquez, P. R. Rela, J. F. T. Martins, J. C. S. M. Pereira, N. Omi, C. H. Mesquita, M. M. Hamada, Gamma-ray computed tomography Scanners for applications in multiphase system columns. *Nukleonika*, v. **54**, p. 129-133, 2009.

10. C. H. Mesquita, P. A. S. Vasquez, M. M. Hamada, Multi-source third generation computed tomography for industrial multiphase flows applications. In: *2011 IEEE Nuclear Science Symposium Conference Record*, Oct. 2011 (in press).

11. C. H. Mesquita, C. C. Dantas, F. E. Costa, D. V. S. Carvalho, T. Madi Filho, P. A. S. Vasquez, M. M. Hamada, Development of a Fourth Generation Industrial Tomography for Multiphase Systems Analysis**.** In*: 2010 IEEE Nuclear Science Symposium Conference Record*, pp. 19-23, Oct. 2010.

12. E. F. Oliveira, S. B. Melo, C. C. Dantas, D. A. A. Vasconcelos, F. Cadiz, Comparison Among Tomographic Reconstruction Algorithms With a Limited Data, *International Nuclear Atlantic Conference - INAC 2011*, 2011, Belo Horizonte. INAC 2011. Belo Horizonte: INAC, 2011.

13. G. Zaddach, *Kernforschusanlage Jülich GmbH – Katalog von Ge (Li)-y-Spektren*, Neuauflage Okt. 1979, ISSN 0366-0885.

14. L. Cadiz, A. Rodrigues, E. O. Oliveira, C. C. Dantas, S. B. Melo, Precisa avaliação da qualidade de imagem reconstruída, *International Nuclear Atlantic Conference - INAC 2009*, Rio de Janeiro, ISSN: 978-85-99141-03-8.

ISBN: **978-85-99141-05-2**

15. E. F. Oliveira, S. B. Melo, C. C. Dantas, I. V. Mota, M. Lira, Tomographic Reconstruction With B-Splines Surfaces, *International Nuclear Atlantic Conference - INAC 2011*, 2011, Belo Horizonte.

16. "X-Ray Mass Attenuation Coefficients – Table 4", http://physics.nist.gov/PhysRefData/XrayMassCoef/tab4.html (2013).

17. "X-Ray Mass Attenuation Coefficients – Table 3", http://physics.nist.gov/PhysRefData/XrayMassCoef/tab3.html (2013).

18. R. Cesareo, A. Brunetti, C. C. Borlino, Et. Al.; X and g-RAY Tomography for the study of works of art, http://www.ndt.net/article/v05n01/cesareo/cesareo.htm, (2013).